



High-Resolution Spinal Motor Mapping Using Thoracic Spinal Cord Stimulation in Patients With Chronic Pain

Ilknur Telkes, PhD, MSc*
 Amir Hadanny, MD[‡]
 Marisa DiMarzio, PhD*
 Girish Chitnis, PhD[§]
 Steven Paniccioli, BS, CNIM^{||}
 Katherine O'Connor, PhD, CNIM^{||}
 Rachael Grey, BS, CNIM^{||}
 Kevin McCarthy, BS, CNIM^{||}
 Olga Khazen, BS*
 Bryan McLaughlin, PhD[§]
 Julie G. Pilitsis, MD, PhD, MBA  *[‡]

*Department of Neuroscience and Experimental Therapeutics, Albany Medical College, Albany, New York, USA; [‡]Department of Neurosurgery, Albany Medical College, Albany, New York, USA; [§]Micro-Leads Medical, Somerville, Massachusetts, USA; ^{||}Nuvasive Clinical Services, San Diego, California, USA

Part of this study was presented at the Congress of Neurological Surgeons 2021 Annual Meeting in Austin, TX, October 16 to 20, 2021. The abstract titled "Feasibility of Spinal Motor Mapping using High-Resolution Spinal Cord Stimulation Paddles in Patients with Chronic Pain" was selected for the Ronald R. Tasker Young Investigator Award and orally presented at the section on Pain Session 1 on October 18, 2021.

Correspondence:

Julie G. Pilitsis, MD, PhD, MBA,
 Charles E. Schmidt College of Medicine,
 Florida Atlantic University,
 777 Glades Rd,
 Boca Raton, FL 33431, USA.
 Email: jpilitsis@health.fau.edu

Received, November 18, 2021.

Accepted, April 11, 2022.

Published Online, July 11, 2022.

© Congress of Neurological Surgeons 2022. All rights reserved.

BACKGROUND: High-resolution spinal cord stimulation (HR-SCS) paddle can stimulate medial-dorsal columns and extend stimulation coverage to the laterally positioned spinal targets.

OBJECTIVE: To investigate the medio-lateral selectivity of an HR-SCS paddle in patients with chronic pain.

METHODS: During standard-of-care spinal cord stimulation (SCS) placement, epidurally evoked electromyography and antidromic dorsal column-evoked potentials were recorded in 12 subjects using an HR-SCS paddle with 8 medio-lateral sites spanning the full epidural width at thoracic T9-12 and a commercial paddle consecutively.

RESULTS: Recruitment maps were aligned with respect to physiological midline which was overlapping with anatomic midline in 10 of 11 cases. Overlapping contacts between the HR-SCS and commercial paddles exhibited similar patterns while HR-SCS demonstrated higher precision targeting of certain dermatomes. Spinal motor maps showed that the lateral contacts triggered stronger responses in medial gastrocnemius, adductor magnus, and tibialis anterior while the medial contacts triggered stronger responses in gluteus maximus and adductor hallucis. The time-locked popliteal fossa responses indicated ipsilateral activation by HR-SCS at the lateral contacts and bilateral activation at the medial contacts with stronger ipsilateral responses.

CONCLUSION: This study is the first to perform high-resolution medio-lateral SCS mapping in patients with chronic pain. These results show promise that HR-SCS may provide additional ipsilateral recruitment within the extremities which improve targeting of focal pain in the lower extremities. Furthermore, this study supports the functional use of intraoperative neuromonitoring as a decision tool to determine physiological midline in thoracic SCS surgeries and provides a full methodological framework.

KEY WORDS: Chronic pain, Dorsal column mapping, EMG, Spinal cord stimulation

Neurosurgery 91:459–469, 2022

<https://doi.org/10.1227/neu.0000000000002054>

Spinal cord stimulation (SCS) has successfully treated chronic extremity pain for many years.^{1–4} However, current SCS methods

have a limited impact on isolated foot, knee, chest wall, groin, and axial low back pain.^{5–7} Recent lines of clinical evidence suggest that, in addition to

ABBREVIATIONS: ADD, adductor magnus; AH, adductor hallucis; BF, bicep femoris; CRPS, complex regional pain syndrome; Cv5, cervical level 5; DC, dorsal column; DH, dorsal horn; DR, dorsal root; EMG, electromyography; GLUT, gluteus maximus; HR-SCS, high-resolution spinal cord stimulation; IONM, intraoperative neuromonitoring; LAH, left adductor hallucis; LMG, left medial gastrocnemius; LPF, left popliteal fossa; MG, medial gastrocnemius; PF, popliteal fossa; RAH, right adductor hallucis; RMG, right medial gastrocnemius; RMS, root mean square; RPF, right popliteal fossa; SCS, spinal cord stimulation; QUAD, quadriceps; TA, tibialis anterior.

Supplemental digital content is available for this article at neurosurgery-online.com

Access the **CNS Spotlight** gallery at cns.org/spotlight or by scanning this QR code using your mobile device.



TABLE 1. Patient Demographics and Clinical Characteristics

Sex (female/male)	7/5
Age (mean ± SD in years)	52.75 ± 14.75
Diagnosis^a	
Neuropathic pain	12
Failed back surgery syndrome	5
Complex regional pain syndrome	2
BMI (mean ± SD)	32.73 ± 5.39
Duration of illness (mean ± SD in years)	7.42 ± 4.32
Level of active contact^a	
T9	3
T10	8
T11	1
Anterior-posterior diameter (mean ± SD in mm)	15.71 ± 2.74
Interpedicular distance (mean ± SD in mm)	19.55 ± 2.10
Dorsal CSF thickness (mean ± SD in mm)	4.39 ± 1.08
Numerical Rating Scale (mean ± SD)	7 ± 2.13
McGill Pain Questionnaire (mean ± SD)	5.58 ± 2.84
Oswestry Disability Index (mean ± SD)	57.90 ± 18.25
Pain Catastrophizing Scale (mean ± SD)	23.08 ± 13.92
Beck Depression Index (mean ± SD)	18.08 ± 12.21

BMI, body mass index; CSF, cerebrospinal fluid; T, thoracic.

^aIndicating the number of patients.

dorsal column (DC) stimulation, lateral spinal cord structures may provide a new mechanism of action and a more selective opportunity to treat focal pain.^{6,8-11} Therapies which mechanistically target the dorsal horn have been noted to provide superior benefit for the treatment of axial low back pain, an affliction far more common than isolated extremity pain.¹²⁻¹⁴ Inhibitory interneurons in the dorsal horn appear to mediate subperception therapy while dorsal root (DR) ganglia stimulation improves focal pain treatment of chronic postsurgical pain and complex regional pain syndrome.^{11,15}

However, accessing the DR ganglia and lateral spinal cord fibers with conventional SCS hardware is fraught with technical and

procedural complications. Conventional paddles provide coverage for approximately 60% of the spinal cord because of thickness and width constraints,¹⁶ and it is not possible to extend therapy to lateral targets, multivertebral levels, or improve selectivity without additional surgical workflow or risks. The physical rigidity of existing technologies often precludes lateral placement because of compression of the nerve roots or lacks the ability to concurrently stimulate the medial targets. To capture greater neuronal recruitment, using high intensity beyond the threshold is not an option without inducing discomfort and side effects because of the diameter of DC fibers and their distance to the stimulation contacts and structure's electrical properties.^{14,17,18}

To overcome these limitations, we have developed a HR-SCS surgical paddle spanning a 14.5-mm width of the epidural space. The paddle is 60% thinner on the edges to enable safe positioning near the lateral spinal cord structures. Here, based on the methods in our previous studies,¹⁹⁻²³ we performed this feasibility study using intraoperative neurophysiological monitoring (IONM) and investigated the epidurally evoked electromyography (EMG) and antidromic DC-evoked potentials by HR-SCS at thoracic levels of T9-12 in patients with chronic pain.

METHODS

Subjects

Twelve patients who were offered standard-of-care SCS for their chronic back and/or leg pain (with/without previous back surgery) were invited to participate in this Institutional Review Board–approved study. Eleven subjects underwent trial thoracic SCS with percutaneous electrodes while 1 subject with paddle electrode. On successful trial (≥50% pain relief based on the Numeric Rating Scale), patients underwent a laminectomy for permanent SCS paddle placement with IONM and participated in this study with written informed consent. The patient demographics and clinical characteristics are presented in Table 1 (Table, Supplemental

TABLE 2. Implant Specifications

Patients	Trial type	SCS system	Column × row ^a	Electrode model	Battery model
P1	Percutaneous	Nevro	2 × 8	Surpass	Omnia NIPG2500
P2	Percutaneous	Medtronic	3 × 5-6-5	Specify	Intellis
P3	Percutaneous	Boston scientific	4 × 8	CoverEdge 32	Wavewriter
P4	Percutaneous	Nevro	2 × 8	Surpass	Omnia NIPG2500
P5	Percutaneous	Nevro	2 × 8	Surpass	Omnia NIPG2500
P6	Percutaneous	Medtronic	3 × 5-6-5	Specify	Intellis
P7	Percutaneous	Medtronic	3 × 5-6-5	Specify	Intellis
P8	Unknown ^b	Abbott	5 × 4	Penta	Proclaim
P9	Percutaneous	Boston scientific	4 × 8	CoverEdge 32	Wavewriter
P10	Percutaneous	Nevro	2 × 8	Surpass	Omnia NIPG2500
P11	Paddle	Nevro	2 × 8	Surpass	Omnia NIPG2500
P12	Percutaneous	Boston scientific	4 × 8	CoverEdge 32	Wavewriter

SCS, spinal cord stimulation.

^aThe number of columns and rows of the commercial paddles.

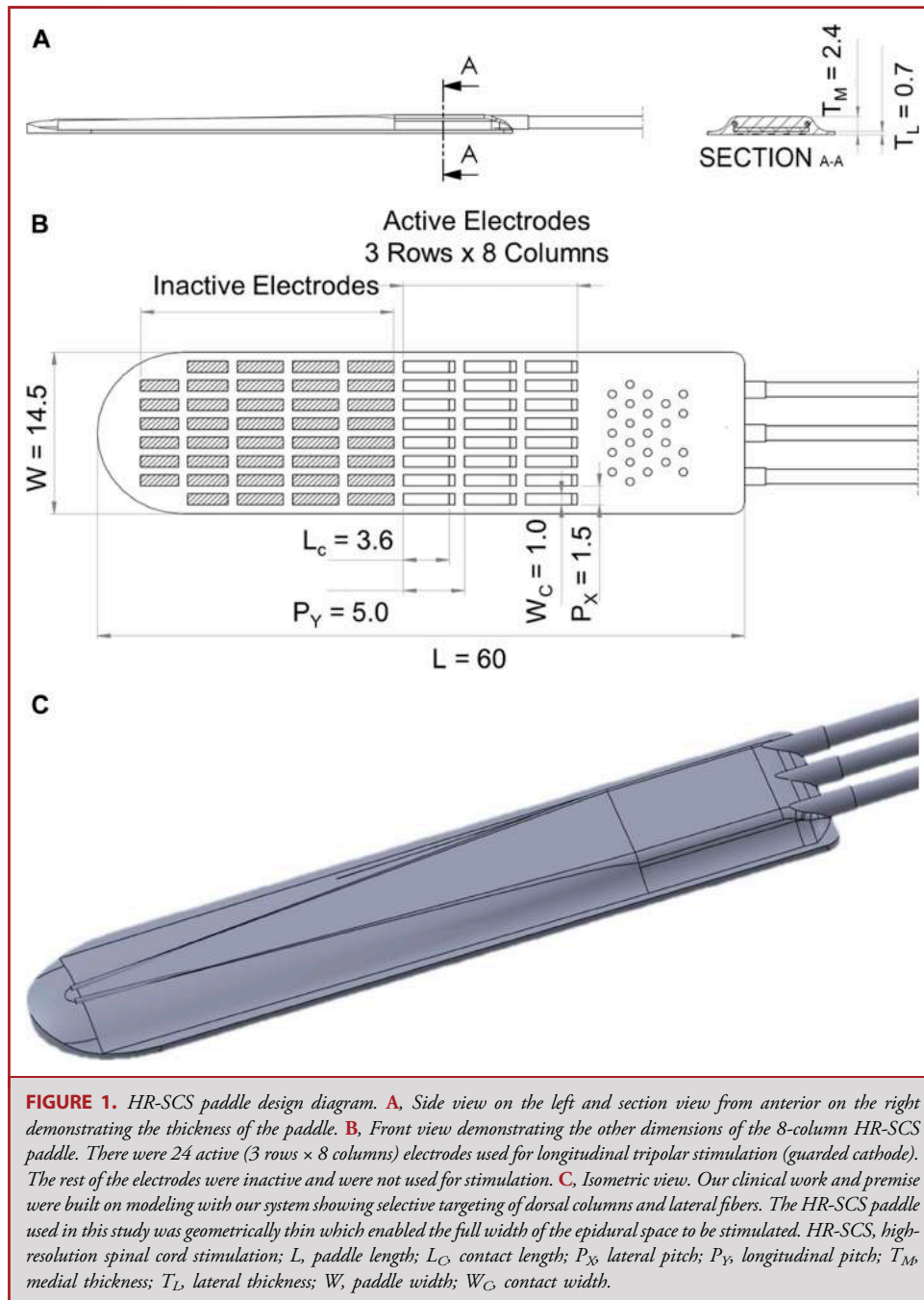
^bTrial was conducted out of Albany Medical center. Trial information is not available. Five patients were implanted with Surpass surgical paddles (Nevro Corp), 3 patients with Specify 5-6-5 (Medtronic Inc), 3 patients with CoverEdge 32 (Boston Scientific), and 1 patient was implanted with Penta paddle (Abbott).

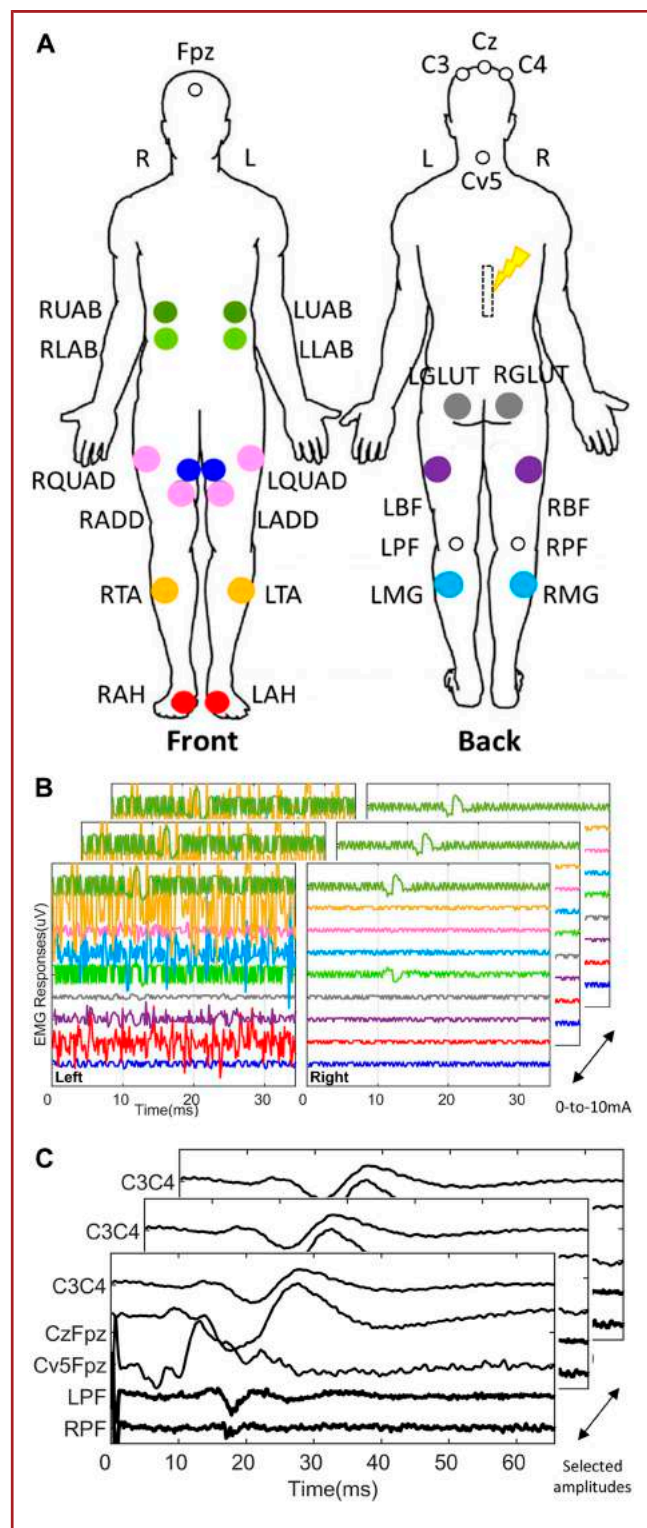
Digital Content 1, <http://links.lww.com/NEU/D211>, for further details). The implant specifications are presented in Table 2.

HR-SCS Paddle Design

A HR-SCS paddle with 8 columns (Micro-Leads Inc) used in this study was designed for investigational purposes. It was designed based on simulation optimizations and the neural activation model of

Holsheimer.^{13,19,24,25} The model was used to compute the DC fiber and DR recruitment profiles using a variety of bipolar, tripolar, and multipolar configurations. The construction used a novel fusion-bond electrode technology to enable thin electrodes with tighter contact spacing. The electrodes were manufactured from platinum-iridium, medical-grade silicone, and nano fibers.¹⁹ Figure 1 presents the design diagram (**Table, Supplemental Digital Content 2**, <http://links.lww.com/NEU/D212>).



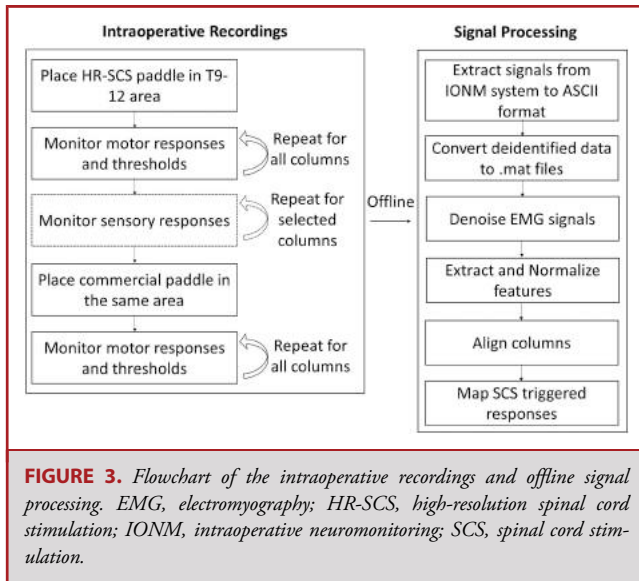


Surgical Placement and Neuromonitoring

A standard-of-care SCS laminectomy was performed under total intravenous anesthesia as previously described (see **Additional Methods, Supplemental Digital Content 3**, <http://links.lww.com/NEU/D213>, for surgical technique).^{20,22} Using serial fluoroscopic imaging, active contacts of HR-SCS paddle were centered over the “sweet spot.”¹⁷ Once the compound muscle action potentials confirmed intact neurological status, HR-SCS paddle was connected to Cascade-Pro IONM systems (Cadwell Inc) for spinal motor mapping.^{20,23} For mapping, as shown in Figure 2A, the following muscle groups were investigated: upper and lower rectus abdominis (upper abdominals, UAB; lower abdominals, LAB), vastus lateralis referenced to vastus medialis (quadriceps, QUAD), adductor magnus (ADD), tibialis anterior (TA), adductor hallucis (AH), gluteus maximus (GLUT), bicep femoris, and medial gastrocnemius (MG).^{20,26} The rostral 3 rows of the HR-SCS paddle were stimulated in a vertical tripole configuration (anode-cathode-anode)^{17,27} at 60 Hz/300 μ s between 0 and 10 mA (Figure 2B).

Ascending sensory responses (Figure 2C) were monitored in the standard electroencephalography positions (Fpz, Cz, C3, and C4) and cervical level 5 while descending responses were captured at the bilateral popliteal fossa (PF). The same active contacts were used at 4.73 Hz with stimulation amplitudes up to 85% of the EMG

FIGURE 2. Intraoperative neuromonitoring setup. **A**, Muscle groups (9 per side) used for spinal motor mapping. Disposable stainless steel subdermal electrodes (13 mm, Rhythmlink) were placed in upper and lower rectus abdominis, vastus lateralis referenced to vastus medialis (quadriceps), adductor magnus, tibialis anterior, adductor hallucis, gluteus maximus, bicep femoris, and medial gastrocnemius muscles. R-/L- indicating right and left side. For cortical sensory testing, needle electrodes were placed in standard 10–20 electroencephalography positions including Fpz, Cz, C3, C4, and cervical level 5. The antidromic dorsal column–evoked potentials were recorded off the tibial nerve at the popliteal fossa. The clear circles representing the sensory channels over the scalp and popliteal fossa channels in the legs. LPF/RPF: left and right popliteal fossa, respectively. **B**, Representation of ipsilateral EMG responses triggered by HR-SCS. Biphasic pulses were delivered at 60 Hz frequency and 300 μ s pulse width while motor responses, and thresholds were recorded using intraoperative neuromonitoring. Each vertical tripole column was tested by stepping up the current from 0 mA with 0.5 mA step size. Stimulation amplitudes varied between 0 and 10 mA. Triggered EMG responses were intraoperatively assessed and recorded for both HR-SCS and commercial paddles. **C**, Representation of SSEPs and popliteal fossa responses triggered by HR-SCS. The same tripolar electrode configuration was used with a stimulation frequency of 4.73 Hz and 300 μ s pulse width using selected amplitudes. Cv5, cervical level 5; EMG, electromyography; HR-SCS, high-resolution spinal cord stimulation; LADD, left adductor magnus; LAH, left adductor hallucis; LBF, left bicep femoris; LGLUT, left gluteus maximus; LLAB, left lower rectus abdominis; LMG, left medial gastrocnemius; LPF, left popliteal fossa; LQUAD, left quadriceps; LTA, left tibialis anterior; LUAB, left upper rectus abdominis; RAH, right adductor hallucis; RADD, right adductor magnus; RBF, right bicep femoris; RGLUT, right gluteus maximus; RLAB, right lower rectus abdominis; RMG, right medial gastrocnemius; RPF, right popliteal fossa; RQUAD, right quadriceps; RTA, right tibialis anterior; RUAB, right upper rectus abdominis.



threshold. Time-locked stimulus averages were performed over 100 trials.²⁸ Owing to time limitation, sensory mapping was performed only for selected columns including most medial and lateral columns on both sides of the anatomic midline.

Once the HR-SCS mapping was complete, based on the final fluoroscopic image of the HR-SCS paddle, commercial paddle was placed at the clinically indicated position and connected to its pulse generator for motor mapping. In 8 cases, the stimulated contacts in both paddles overlapped. In cases where 2 paddles did not align, IONM data were obtained using the most rostral contacts of the commercial paddles. Fluoroscopy was used to determine the anatomic midline position for both paddles (**Supplemental Figure 4, Part A**, <http://links.lww.com/NEU/D214>, **part B**, <http://links.lww.com/NEU/D215>, **part C**, <http://links.lww.com/NEU/D216>). The surgery was completed in a standard fashion.^{20,22}

Signal Processing

All signals were processed offline in MATLAB (MathWorks) as previously described²³ (Figure 3). The EMG signals were denoised using an in-house developed algorithm.²³ Signal's root mean square (RMS) was computed at each amplitude and normalized to baseline (stimulation-OFF). Sensory signals averaged during IONM were analyzed offline without further preprocessing. Previous studies have shown that 80% to 90% of the ionic current flows between active electrodes through the cerebrospinal fluid (CSF) during epidural stimulation.^{29,30} Based on these and our previous work³¹ showing a relationship between postoperative energy requirements, we hypothesized that the size of the canal and the CSF thickness may have a role in recording amplitudes. Therefore, peak-to-peak amplitudes of the response latency were calculated^{31,32} and analyzed against patient's spinal column and CSF measurements (see **Additional Methods, Supplemental Digital Content 3**, <http://links.lww.com/NEU/D213>, for anatomic measurements).

Due to anatomic constraints that limited relative paddle positioning in some cases, contact positions were aligned offline based on fluoroscopy

and IONM. Because a single contact of HR-SCS paddle was 1 mm in width, the same distance was used for electrode clustering (**Supplemental Figure 5**, <http://links.lww.com/NEU/D217>). Specifically, a column positioned at the anatomic midline was labeled as "0." The left-sided columns were labeled negative, and right-sided columns were labeled positive. Both paddles were aligned in the same fashion. In 1 case, physiological midline differed from anatomic midline and the alignment of midline was modified slightly based on these data.

Statistical Analysis

Statistical analyses were performed in IBM SPSS Statistics (version-22). To assess the left-to-right symmetry, ipsilateral evoked EMGs were compared using the two-tailed Mann-Whitney *U* test. A Kruskal-Wallis test was then used to compare the laterality and selectivity of motor and sensory responses. To determine the correlation between the HR-SCS and commercial paddle, the Pearson χ^2 test of independence was conducted. Multiple comparisons were adjusted using Bonferroni correction. Association between PF responses and MRI-based features were evaluated using Spearman rank correlation coefficient. The weighted categorical distributions of PFs were compared across contacts by using the Pearson χ^2 test. An $\alpha < 0.05$ was considered for statistical significance.

RESULTS

Our cohort included patients with neuropathic pain ($n = 12$) with average diagnosis of 7.42 ± 4.32 years. The demographics and clinical characteristics are presented in Table 1. The commercial implant specifications per subject are presented in Table 2. Due to failure to save an intraoperative image of the HR-SCS paddle in 1 case, it was not possible to align the tested contacts during the offline analysis. Therefore, the patient was excluded from further analysis.

Motor Mapping

The spatial coverage and stimulation selectivity of the HR-SCS paddle was compared with commercial paddles by quantifying the changes in motor responses. Figure 4A and 4B shows motor activity maps in a representative patient. Individual heatmaps provide rapid visualization of laterality in the responses. Stimulation of column-1 induced stronger lower extremity responses, left adductor hallucis (LAH), left tibialis anterior (LTA), and left medial gastrocnemius (LMG) while column-8 induced strong ipsilateral responses in right adductor hallucis (RAH), right tibialis anterior (RTA), right medial gastrocnemius (RMG), and right upper rectus abdominis (RUAB).

Figure 5A and 5B illustrates the recruitment plots for bilateral AH and MG at all tested amplitudes. Ipsilateral muscles in both cases showed stronger physiological responses. When the responses above the decision threshold were averaged to obtain a single outcome metric, a similar selectivity pattern was noted (Figure 5C and 5D). Particularly, LAH indicated a gradual increase toward midline and RAH responses in columns 5 and 8 were comparable. The maximum LMG and RMG activities were noted in columns 3 and 6.

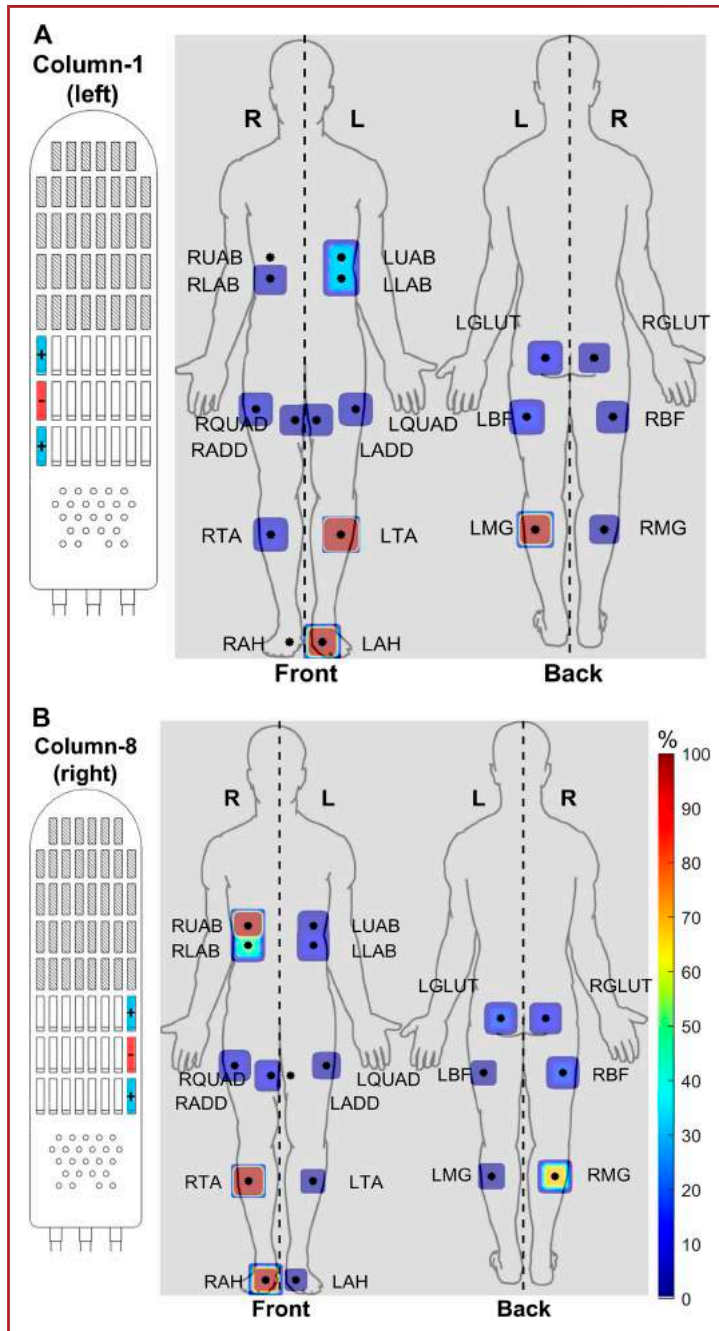


FIGURE 4. SCS-triggered activity maps. Heatmaps representing normalized RMS values of triggered EMGs when stimulation was delivered from **A**, column-1, left lateral, and **B**, column-8, right lateral. The stimulation amplitude is 6 mA. Color bar indicating the stimulation-induced changes with respect to baseline in percentage (%). EMG, electromyography; LADD, left adductor magnus; LAH, left adductor hallucis; LGLUT, left gluteus maximus; LLAB, left lower rectus abdominis; LMG, Left medial gastrocnemius; LPF, left popliteal fossa; LQUAD, left quadriceps; LTA, left tibialis anterior; LUAB, left upper rectus abdominis; RADD, right adductor magnus; RAH, right adductor hallucis; RGLUT, right gluteus maximus; RLAB, right lower rectus abdominis; RMG, right medial gastrocnemius; RMS, root mean square; RPF, right popliteal fossa; RQUAD, right quadriceps; RTA, right tibialis anterior; RUAB, right upper rectus abdominis; SCS, spinal cord stimulation.

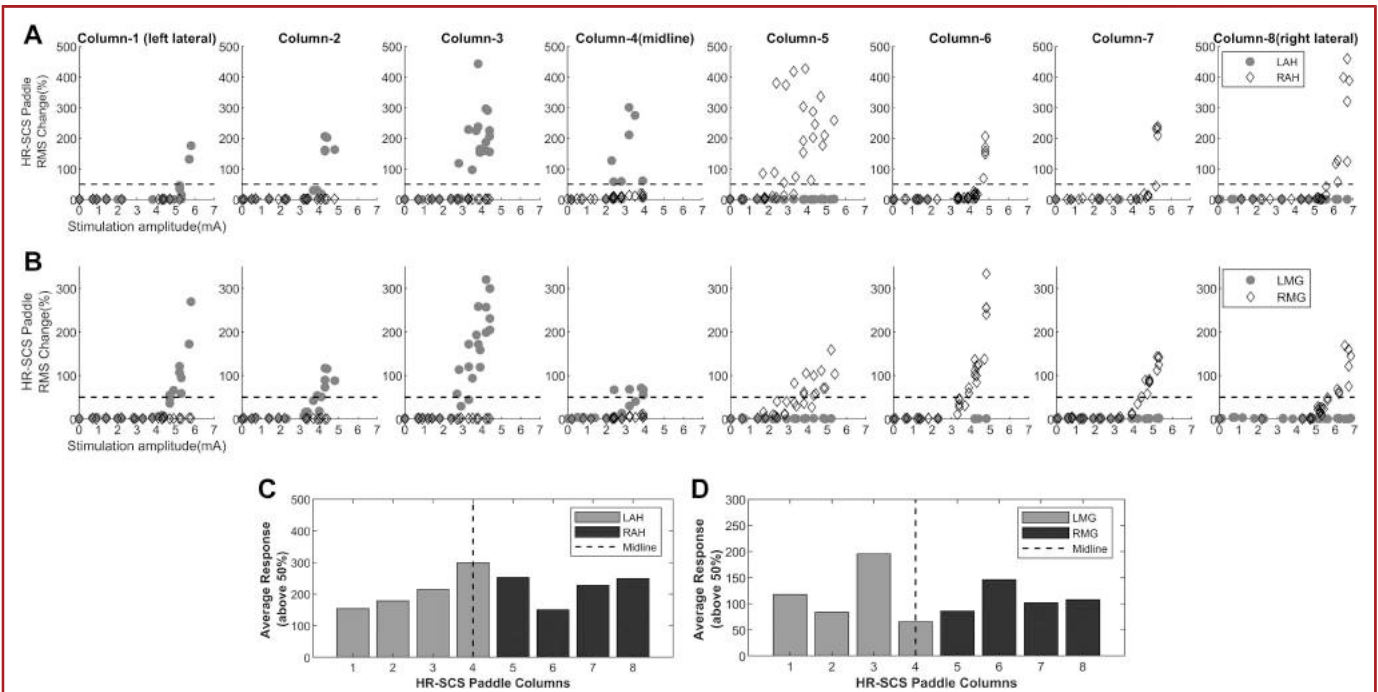


FIGURE 5. EMG recruitment plots. Distribution of the normalized root mean square values of spinal cord stimulation–triggered EMGs at all tested amplitudes in a representative subject across all columns in **A**, AH and **B**, MG. Tested columns are shown from the left lateral to medial to the right lateral. Gray circles: left side responses (LAH and LMG). Black diamonds: right side responses (RAH and RMG). Black dashed lines indicating decision threshold at 50% change with respect to baseline. Laterality was defined in our intraoperative neuromonitoring protocol for identification of the physiological midline when the ipsilateral EMG was two times larger than the EMG responses on the contralateral side. The anatomic midline was used to assess laterality offline and grouped the columns as left vs right with respect to the midline accordingly. Average physiological responses (values above the decision threshold) in **C**, AH and **D**, MG muscles per column. Anatomic midline is shown with a dashed line. Gray bars: left side. Black bars: right side. AH, adductor hallucis; EMG, electromyography; HR-SCS, high-resolution spinal cord stimulation; LAH, left adductor hallucis; LMG, left medial gastrocnemius; MG, medial gastrocnemius; RAH, right adductor hallucis; RMG, right medial gastrocnemius.

The ipsilateral EMGs captured by left-sided and right-sided columns located the same distance away from physiological midline did not show a significant difference ($P > .05$); thus, the columns with the same distance to the midline were combined for further analysis. The recruitment maps showed similar patterns between HR-SCS and commercial paddles over the overlapped columns while the distal columns of the HR-SCS paddle exhibited distinct responses because of its higher spatial resolution. Figure 6 shows the response distribution of both paddles. Lateral HR-SCS triggered stronger responses in ADD, MG, TA, and QUAD while medial HR-SCS triggered higher activation in GLUT and AH. Despite the lower spatial resolution in commercial paddles, the overlapping contacts with the HR-SCS paddle showed similar mediolateral trends in ADD, QUAD, GLUT, and AH. Statistical analysis showed significant differences in MG ($H(4) = 9.93$, $P = .041$) and marginal differences in TA ($H(4) = 8.57$, $P = .072$). Despite the trends between lateral and medial columns, the adjusted pairwise comparisons did not show a significant difference ($P > .005$). Laterality was not observed in the abdominal muscles (upper and lower rectus abdominis) in either condition (see **Supplemental Figure 6**, <http://links.lww.com/NEU/D218>

and **Supplemental Figure 7**, <http://links.lww.com/NEU/D219>, for details of stimulation amplitudes).

Sensory Mapping

Figure 7A and 7B shows ipsilateral and contralateral PF responses obtained in a representative patient. Left lateral column triggered stronger left PF while both medial columns evoked strong ipsilateral PFs. The categorical comparison of PFs (Figure 7C, **Figure, Supplemental Digital Content 8**, <http://links.lww.com/NEU/D220>) showed that medial columns triggered more responses (left: 8/10 and right: 7/10). Stimulation of the lateral columns induced only ipsilateral responses. Statistical analysis indicated a significant association between location and PFs (left: $\chi^2[7, N = 48] = 16.59$, $P = .020$; right: $\chi^2[7, N = 48] = 20.21$, $P = .005$). However, significance did not hold following the Bonferroni correction (corrected $P = .003$). Comparison between combined columns also showed a significant association with PFs (left: $\chi^2[4, N = 48] = 12.89$, $P = .012$; right: $\chi^2[4, N = 48] = 18.71$, $P = .001$); however, Bonferroni correction showed no significance (corrected $P = .005$). Spearman correlation analysis did not show significant correlation between the MRI-based features and PFs (**Supplemental**

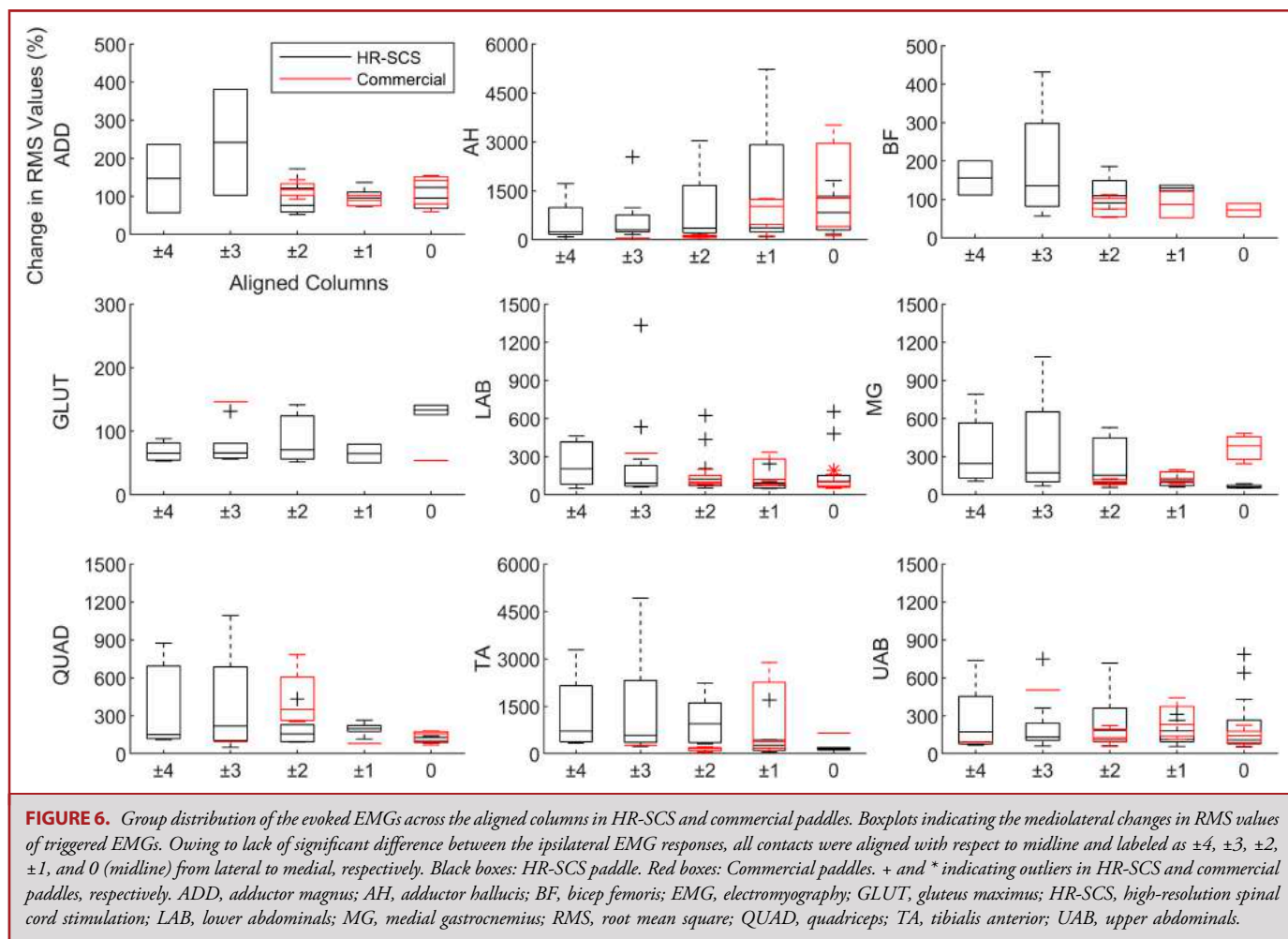


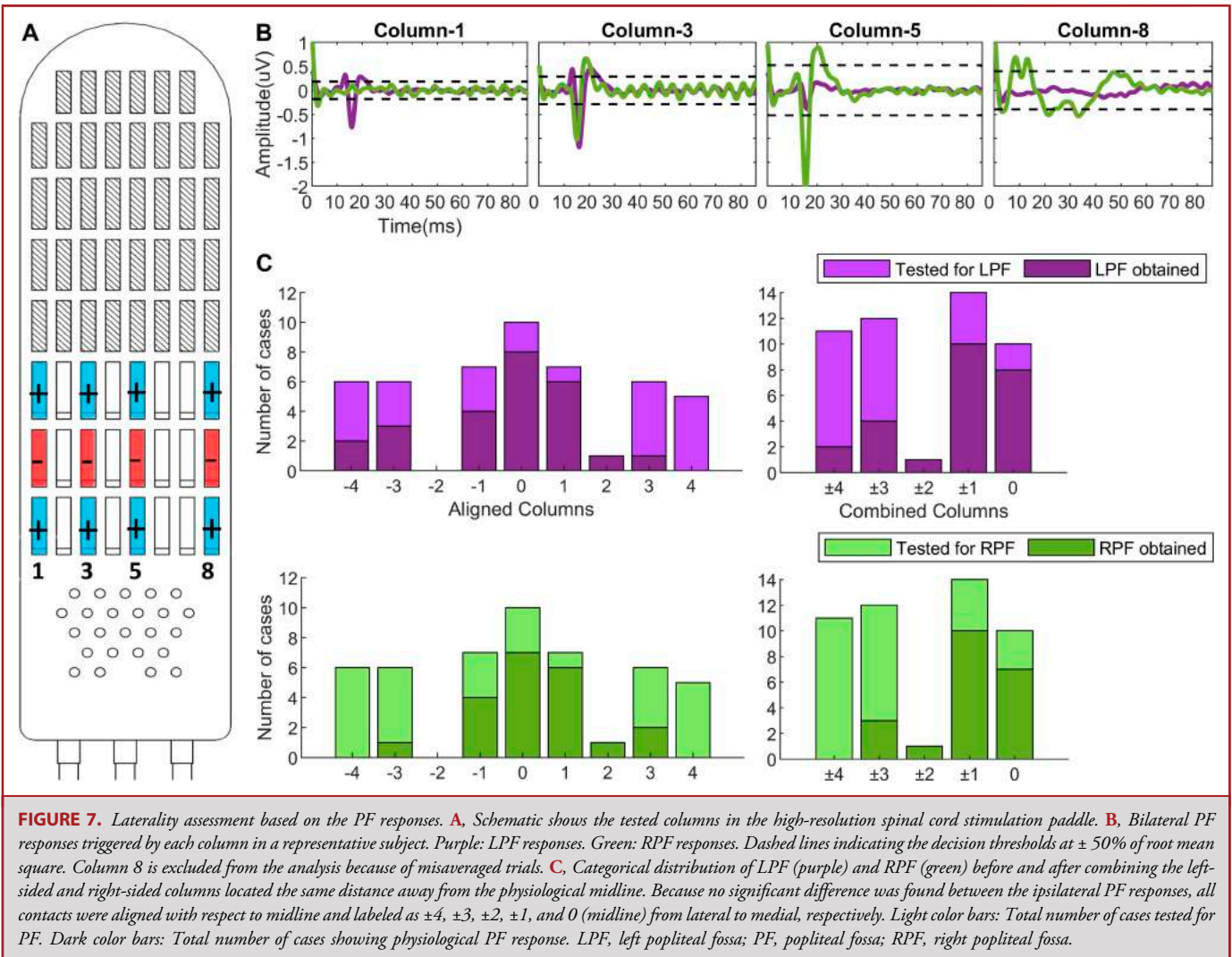
Figure 9A, <http://links.lww.com/NEU/D221>, <http://links.lww.com/NEU/D222>, **9B, 9C,** <http://links.lww.com/NEU/D223>).

DISCUSSION

In this National Institutes of Health–Helping to End Addiction Long-term (NIH-HEAL) initiative study, we tested the feasibility of using a HR-SCS paddle for spinal motor mapping. We investigated the activation of medial and lateral thoracic targets using IONM in patients with chronic pain and compared the spatial coverage of the HR-SCS paddle with commercially available paddles. We were able to show patterns of mediolateral recruitment of the leg, foot, and buttock muscles in addition to antidromic DC sensory–evoked potentials. This study is unique in the sense of mapping intraoperative motor and antidromic sensory activity using various locations over T9–12 of spinal cord in humans and comparing recruitment maps of HR-SCS paddles with commercial paddles in the same subjects.

To cover the low back pain, stimulation is delivered to reach the DC fibers located deep in the area by avoiding from stimulating DR fibers.³³ Because the T9–10 also have fibers representing the buttock and anterior legs, stimulation of DC produces more widespread paresthesia unlike DR stimulation where paresthesia is usually induced at a single dermatome.^{12,34} Therefore, accurate placement of SCS electrode is important to avoid from inducing stimulation-induced side effects. Although spinal cord mapping has been widely investigated in animals, human mapping has been limited. Recently, Hofstoetter et al³⁵ constructed longitudinal (top-down) mapping between the anatomic stimulated site and the activated spinal segments. The correlation between the anatomic stimulation site and the activated medial-to-lateral DC has yet to be investigated. This study is the first study in the literature to perform medial-to-lateral mapping at T9–12 in patients with chronic pain, where the stimulation pattern was in accordance with the spatial organization of DC fibers.¹⁸

The activity maps demonstrated higher spatial recruitment by HR-SCS. Both paddles showed the same level of response in



upper leg (ADD, BF) and lower extremity muscles (AH and MG) with medial stimulation; however, only HR-SCS through lateral stimulation induced physiological responses in these muscles. Considering that the HR-SCS paddle is 5- to 7-mm wider than the 2-to-5-column commercial paddles, it is reasonable to expect wider lateral recruitment. Although similar activation patterns were observed in overlapping contacts between the paddles, additional lateral contacts in the HR-SCS paddle targeted extremity muscles selectively. It is possible that the additional ipsilateral control within the extremities of the HR-SCS may lead to improved targeting of focal pain in the lower (and possibly upper) extremities.^{11,15}

The commercial paddles with fewer, coarsely spaced columns provide some buffer to overcome discrepancies between anatomic and physiological midline up to 2 mm. However, if the subject had unilateral or focal pain, the commercial paddle would be less likely to cover the painful area. Higher amplitudes may reach these

targets; however, they would result in off-target discomfort and carry the risk of draining the battery sooner. Therefore, as our group demonstrated previously,³¹ determining the physiological midline properly during the surgery using IONM might provide an optimal lead placement for greatest efficacy and a priori knowledge on postoperative programming.

This pilot study demonstrates the feasibility of using HR-SCS paddles in human subjects to provide selective stimulation and to treat a wider area of the spinal cord and the associated dermatomes. HR-SCS provides 50% wider stimulation area including DC, rootlets, and DR. By providing comprehensive coverage of the spinal cord, the need for intraoperative/awake-patient testing to identify proper placement might be eliminated, because the full epidural width is treatable by a single electrode array. Furthermore, the span of the paddle provides a new ability to selectively stimulate discrete DR fibers for more selective treatment of focal pain including complex regional pain syndrome, postherniorrhaphy, and knee pain.^{11,15}

We demonstrated that selective recruitment could be accomplished in many subjects which could not be performed using conventional paddles. The programming of HR-SCS paddles would be performed using a semiautomated algorithm which localizes stimulation to a larger area and then with patient feedback focuses the stimulation to a narrower range of dermatomes. Our ultimate goal is to test HR-SCS in awake patients who can report localization of paresthesia and quality of pain therapy in a particular dermatome. These long-term studies would help determine whether the HR-SCS paddles may one day replace conventional paddles.

Limitations of the Study

We acknowledge several limitations of this feasibility study. First, our sample size was limited to 11 patients with complete data. Second, this study was limited to 25-minute monitoring under general anesthesia; thus, data collection was limited to certain decisions. Third, recruitment of PFs from the commercial paddles was not possible because of lack of a commercially available adaptor to connect to the IONM system. Finally, both our HR-SCS paddle and commercial paddles were not placed at the exact same location in all cases. We mitigated this limitation by aligning all stimulation contact sets to the anatomic midline based on intraoperative x-ray images.

CONCLUSION

Our results showed that HR-SCS was able to evoke distinct motor responses at thoracic levels and exhibited unique patterns in the lower extremities. Although there is no postoperative paresthesia mapping in this study, we speculate that wider spatial coverage of HR-SCS paddle might simultaneously target lower back and distal extremity pain and be an alternative to more challenging surgeries. Furthermore, our study supports the functional use of IONM in SCS surgery and provides a robust methodological framework.

Funding

This work has been funded by Micro-Leads through NIH Award U44NS115111. Dr Pilitsis receives grant support from Medtronic, Boston Scientific, Abbott, Nevro, Micro-Leads (U44NS115111), and NIH 2R01CA166379-06. Dr Telkes has received grant support from Micro-Leads (U44NS115111) and NIH K99NS119672. Dr Hadanny is supported by a fellowship sponsored by Medtronic, Boston Scientific, and Abbott.

Disclosures

Dr Pilitsis is a consultant for Boston Scientific, Nevro, Medtronic, Saluda, and Abbott and is the medical advisor for Aim Medical Robotics. Dr Hadanny had stock equity in Aviv Scientific and EEG-Sense. Bryan McLaughlin and Girish Chitnis are employees of Micro-leads Medical. Steven Paniccioli, Katherine O'Connor, Rachael Grey, and Kevin McCarthy are employees of Nuvasive Clinical Services.

REFERENCES

1. Gee L, Smith HC, Ghulam-Jelani Z, et al. Spinal cord stimulation for the treatment of chronic pain reduces opioid use and results in superior clinical outcomes when used without opioids. *Neurosurgery*. 2019;84(1):217-226.

2. Sharan AD, Riley J, Falowski S, et al. Association of opioid usage with spinal cord stimulation outcomes. *Pain Med*. 2018;19(4):699-707.
3. Cameron T. Safety and efficacy of spinal cord stimulation for the treatment of chronic pain: a 20-year literature review. *J Neurosurg*. 2004;100(3 suppl spine):254-267.
4. Van Buyten JP, Van Zundert J, Vueghs P, Vanduffel L. Efficacy of spinal cord stimulation: 10 years of experience in a pain centre in Belgium. *Eur J Pain*. 2001; 5(3):299-307.
5. Deer T, Pope J, Hayek S, et al. Neurostimulation for the treatment of axial back pain: a review of mechanisms, techniques, outcomes, and future advances. *Neuromodulation*. 2014;17(suppl 2):52-68.
6. Schu S, Gulve A, ElDabe S, et al. Spinal cord stimulation of the dorsal root ganglion for groin pain—a retrospective review. *Pain Pract*. 2015;15(4):293-299.
7. De La Cruz P, Fama C, Roth S, et al. Predictors of spinal cord stimulation success. *Neuromodulation*. 2015;18(7):599-602; discussion 602.
8. Liem L, Russo M, Huygen FJ, et al. A multicenter, prospective trial to assess the safety and performance of the spinal modulation dorsal root ganglion neurostimulator system in the treatment of chronic pain. *Neuromodulation*. 2013;16(5): 471-482; discussion 482.
9. Liem L, Mekhail N. Management of postherniorrhaphy chronic neuropathic groin pain: a role for dorsal root ganglion stimulation. *Pain Pract*. 2016;16(7):915-923.
10. Van Buyten JP, Smet I, Liem L, Russo M, Huygen F. Stimulation of dorsal root ganglia for the management of complex regional pain syndrome: a prospective case series. *Pain Pract*. 2015;15(3):208-216.
11. Deer TR, Levy RM, Kramer J, et al. Dorsal root ganglion stimulation yielded higher treatment success rate for complex regional pain syndrome and causalgia at 3 and 12 months: a randomized comparative trial. *Pain*. 2017;158(4): 669-681.
12. Oakley JC. Spinal cord stimulation in axial low back pain: solving the Dilemma. *Pain Med*. 2006;7(suppl_1):S58-S63.
13. Holsheimer J, Buitenweg JR. Review: bioelectrical mechanisms in spinal cord stimulation. *Neuromodulation*. 2015;18(3):161-170; discussion 170.
14. Jensen MP, Brownstone RM. Mechanisms of spinal cord stimulation for the treatment of pain: still in the dark after 50 years. *Eur J Pain*. 2019;23(4):652-659.
15. Deer TR, Pope JE, Lamer TJ, et al. The neuromodulation appropriateness consensus committee on best practices for dorsal root ganglion stimulation. *Neuromodulation*. 2019;22(1):1-35.
16. Walker J. When spine implants cause paralysis, who is to blame? *Wall Street Journal*. April 15, 2014.
17. Sheldon B, Staudt MD, Williams L, Harland TA, Pilitsis JG. Spinal cord stimulation programming: a crash course. *Neurosurg Rev*. 2021;44(2):709-720.
18. Feirabend HK, Choufoer H, Ploeger S, Holsheimer J, van Gool JD. Morphometry of human superficial dorsal and dorsolateral column fibres: significance to spinal cord stimulation. *Brain*. 2002;125(pt 5):1137-1149.
19. McLaughlin BL, Buitenweg JR, Stelwagen TJ, Barolat G. *Improved Targeting of Lateral Dorsal Columns With a 64-contact, Current-steering Paddle for Axial Low-Back Pain*. Presented at: North American Neuromodulation Society; 2017.
20. Roth SG, Lange S, Haller J, et al. A prospective study of the intra- and postoperative efficacy of intraoperative neuromonitoring in spinal cord stimulation. *Stereotact Funct Neurosurg*. 2015;93(5):348-354.
21. Mammis A, Mogilner AY. The use of intraoperative electrophysiology for the placement of spinal cord stimulator paddle leads under general anesthesia. *Neurosurgery*. 2012;70(2 suppl operative):230-236.
22. Air EL, Toczyl GR, Mandybur GT. Electrophysiologic monitoring for placement of laminectomy leads for spinal cord stimulation under general anesthesia. *Neuromodulation*. 2012;15(6):573-580; discussion 579-580.
23. Telkes I, Behal A, Hadanny A, et al. Rapid visualization tool for intraoperative dorsal column mapping triggered by spinal cord stimulation in chronic pain patients. In: *Annual International Conference of the IEEE Engineering in Medicine and Biology Society*. Vol 2021. 2021:5760-5763.
24. Holsheimer J, Barolat G. Spinal geometry and paresthesia coverage in spinal cord stimulation. *Neuromodulation*. 1998;1(3):129-136.
25. Sankarasubramanian V, Buitenweg JR, Holsheimer J, Veltink P. Performance of transverse tripoles vs. longitudinal tripoles with anode intensification (AI) in spinal cord stimulation: computational modeling study. *Neuromodulation*. 2014;17(5): 457-464; discussion 463-464.
26. Shils JL, Arle JE. Intraoperative neurophysiologic methods for spinal cord stimulator placement under general anesthesia. *Neuromodulation*. 2012;15(6):560-571; discussion 571-572.

27. Holsheimer J, Wesslink WA. Effect of anode–cathode configuration on paresthesia coverage in spinal cord stimulation. *Neurosurgery*. 1997;41(3):654-659; discussion 659-660.
28. MacDonald DB, Dong C, Quatral R, et al. Recommendations of the International Society of Intraoperative Neurophysiology for intraoperative somatosensory evoked potentials. *Clin Neurophysiol*. 2019;130(1):161-179.
29. Holsheimer J. Concepts and methods in neuromodulation and functional electrical stimulation: an introduction. *Neuromodulation*. 1998;1(2):57-61.
30. Holsheimer J. Which neuronal elements are activated directly by spinal cord stimulation. *Neuromodulation*. 2002;5(1):25-31.
31. Collison C, Prusik J, Paniccioli S, et al. Prospective study of the use of intraoperative neuromonitoring in determining post-operative energy requirements and physiologic midline in spinal cord stimulation. *Neuromodulation*. 2017;20(6):575-581.
32. Larsen JL. The lumbar spinal canal in children. Part II: the interpedicular distance and its relation to the sagittal diameter and transverse pedicular width. *Eur J Radiol*. 1981;1(4):312-321.
33. Howell B, Lad SP, Grill WM. Evaluation of intradural stimulation efficiency and selectivity in a computational model of spinal cord stimulation. *PLoS One*. 2014; 9(12):e114938.
34. North RB, Fowler K, Nigrin DJ, Szymanski R. Patient-interactive, computer-controlled neurological stimulation system: clinical efficacy in spinal cord stimulator adjustment. *J Neurosurg*. 1992;76(6):967-972.
35. Hofstoetter US, Perret I, Bayart A, et al. Spinal motor mapping by epidural stimulation of lumbosacral posterior roots in humans. *iScience*. 2021;24(1):101930.

Acknowledgments

We would like to thank Christina Taylor of Nevro Corporation, Jared Bench of Medtronic Inc., Christopher Bigelow of Boston Scientific Corporation, and Liam McCarthy of Abbott Corporation for their contributions to this work.

The *CNS Spotlight* gallery is available at cns.org/spotlight.

Supplemental digital content is available for this article at neurosurgery-online.com

Supplemental Digital Content 1. Table. Subject demographics with individual values.

Supplemental Digital Content 2. Table. Specifications of high-resolution spinal cord stimulation paddle.

Supplemental Digital Content 3. Additional Methods. Surgical technique and anatomic measurements.

Supplemental Digital Content 4. Figure. Intraoperative X-ray images of the high-resolution spinal cord stimulation (HR-SCS) paddles overlaid with commercial paddles in 3 representative subjects. Overlay with a 2-column commercial paddle **A**, a 4-column commercial paddle **B**, and a 3-column commercial paddle **C**. The tripolar contacts tested for mapping demonstrate a good overlap in cases **A** and **B** while it is suboptimal in case **C**. Here, the most caudal contacts were used for mapping. All paddles were placed over thoracic T9-10.

Supplemental Digital Content 5. Figure. Electrode clustering. As shown in the intraoperative x-ray image of a representative subject, anatomic midline was determined, and the columns (tripolar contact sets) positioned at this midline was relabeled as “0.” The columns on the left with respect to midline were relabeled as -1 , -2 , -3 , and -4 , from medial to lateral, respectively. Similarly, the columns

on the right with respect to midline were relabeled as $+1$, $+2$, $+3$, and $+4$, from medial to lateral, respectively.

Supplemental Digital Content 6. Figure. Distribution of the high-resolution spinal cord stimulation (HR-SCS) amplitudes used in motor mapping. Color bar indicates the maximum current levels used for mapping in all subjects across the columns. *representing the anatomic midline. Owing to failure in capturing the intraoperative x-ray image of the study electrode, no midline is marked in Subject 10. Mapping started at 0 mA, and the stimulus amplitude was increased in 0.5 mA steps until neuromonitoring identified an activation threshold. The maximum amplitude was limited to 10 mA similar to the clinical standard of care. Heatmap demonstrates the maximum pulse amplitudes used in each column across subjects. In 4 subjects, the maximum amplitudes reached to 10 mA in all mediolateral locations, while in 2 subjects, the test was stopped at maximum 3 mA and 7 mA, respectively, where a motor threshold was reached. In other subjects, the maximum levels varied between 6 and 10 mA. When the recruitment maps were examined for the amplitudes triggered an initial physiological response, trends showed that lateral targets in comparison with medial targets required higher amplitudes to evoke response in adductor hallucis (AH) (mean \pm SD = 7 ± 3.16 mA vs 3.08 ± 2.62 mA) and gluteus maximus (GLUT) (6.75 ± 4.27 mA vs 4 ± 0 mA) while the medial targets required higher amplitudes to evoke response in adductor magnus (ADD) (8.5 ± 0.71 mA vs 5 ± 5.66 mA) and tibialis anterior (TA) (7.5 ± 2.12 mA vs 5 ± 3.56 mA) in comparison with lateral targets. However, statistical analyses did not show significant difference in any of the muscles ($P > .05$).

Supplemental Digital Content 7. Figure. Distribution of the stimulation amplitudes triggered physiological response in high-resolution spinal cord stimulation (HR-SCS). Boxplots indicating stimulation amplitudes that correspond to the first value exceeding the decision threshold (50% change). Columns labeled as ± 4 , ± 3 , ± 2 , ± 1 , and 0 are from lateral to medial, respectively. Black lines with circles indicating the group mean and the + indicating outliers. ADD, adductor magnus; AH, adductor hallucis; BF, bicep femoris; GLUT, gluteus maximus; LAB, lower rectus abdominis; MG, medial gastrocnemius; QUAD, quadriceps; TA, tibialis anterior; UAB, upper rectus abdominis.

Supplemental Digital Content 8. Figure. Left popliteal fossa (LPF) responses with respect to stimulation at different amplitudes (1-5.5 mA) and locations (columns 1, 3, 5, and 8). For categorical comparison of popliteal fossa (PF) responses over the mediolateral columns, the following decision criteria applied: (i) a threshold was set to $\pm 50\%$ of the signal's root mean square (RMS) and (ii) any peak appearing >10 ms later than stimulation onset and passing the threshold was considered as physiological PF response. An initial visual assessment was conducted to exclude the corrupted signals (eg, high deviation, contaminated trials). Black dashed lines indicating the decision thresholds at $\pm 50\%$ of RMS. Dashed lines in magenta indicating the 10-millisecond time point after stimulation onset.

Supplemental Digital Content 9. Figure. Correlation between MRI-based features and peak latency of ipsilateral PF responses. **A**, Peak latency in millisecond vs anterior-posterior diameter of dorsal column in mm. **B**, Peak latency in millisecond vs interpedicular distance in mm. **C**, Peak latency in millisecond vs dorsal cerebrospinal fluid (CSF) thickness in mm. Columns labeled as -4 , -3 , and -1 are from left lateral to medial, respectively. Columns labeled as $+4$, $+3$, and $+1$ are from right lateral to medial, respectively. Column labeled as 0 is the midline. Spearman correlation analysis did not show significant correlation between features.